Toxicology 332 (2015) 52–66

Contents lists available at ScienceDirect

Toxicology

journal homepage: www.elsevier.com/locate/toxicol

Use of in vitro data in developing a physiologically based pharmacokinetic model: Carbaryl as a case study

Miyoung Yoon[a,*], Gregory L. Kedderis[b], Grace Zhixia Yan[a], Harvey J. Clewell III[a]

[a] Center for Human Health Assessment, The Hamner Institutes for Health Sciences, Research Triangle Park, NC, USA
[b] Independent Consultant, Chapel Hill, NC, USA

ARTICLE INFO

Article history:
Received 21 May 2013
Received in revised form 2 April 2014
Accepted 18 May 2014
Available online 24 May 2014

Keywords:
Carbaryl
Metabolism
PBPK model
In vitro to in vivo extrapolation
Hepatocytes
Cholinesterase inhibition

ABSTRACT

In vitro-derived information has been increasingly used to support and improve human health risk assessment for exposure to chemicals. Physiologically based pharmacokinetic (PBPK) modeling is a key component in the movement toward in vitro-based risk assessment, providing a tool to integrate diverse experimental data and mechanistic information to relate in vitro effective concentrations to equivalent human exposures. One of the challenges, however, in the use of PBPK models for this purpose has been the need for extensive chemical-specific parameters. With the remarkable advances in in vitro methodologies in recent years, in vitro-derived parameters can now be easily incorporated into PBPK models. In this study we demonstrate an in vitro data based parameterization approach to develop a physiologically based pharmacokinetic and pharmacodynamic (PBPK/PD) model, using carbaryl as a case study. In vitro experiments were performed to provide the chemical-specific pharmacokinetic (PK) and pharmacodynamic (PD) parameters for carbaryl in the PBPK model for this compound. Metabolic clearance and cholinesterase (ChE) interaction parameters for carbaryl were measured in rat and human tissues. These in vitro PK and PD data were extrapolated to parameters in the whole body PBPK model using biologically appropriate scaling. The PBPK model was then used to predict the kinetics and ChE inhibition dynamics of carbaryl in vivo. This case study with carbaryl provides a reasonably successful example of utilizing the in vitro to in vivo extrapolation (IVIVE) approach for PBPK model development. This approach can be applied to other carbamates with an anticholinesterase mode of action as well as to environmental chemicals in general with further refinement of the current shortcomings in the approach. It will contribute to minimizing the need for in vivo human data for PBPK model parameterization and evaluation in human risk assessments.

1. Introduction

Recently, a great deal of attention has been focused on promoting the use of in vitro and in silico approaches to improve risk and safety assessment of chemicals (Andersen and Krewski, 2010; Judson et al., 2011; Knudsen et al., 2011). While this new direction toward in vitro-based risk assessment has the promise to provide more mechanism-based assessment of adverse effects of chemicals in a high throughput manner, one of the challenges is the interpretation of toxicity data from cellular assays in the context of human exposures. Pharmacokinetic modeling plays a critical role in that interpretation by providing a tool to relate the in vitro point of departure concentration to external dose to humans from environmental exposure (Basketter et al., 2012; Blaauboer, 2010; Rotroff et al., 2010; Wetmore et al., 2012; Yoon et al., 2012a). In this process, referred to as quantitative in vitro to in vivo extrapolation (QIVIVE), the in vitro concentration is first related to the equivalent target tissue concentration, using blood concentration as a surrogate, and then the external dose that could achieve that concentration at steady state is estimated through reverse dosimetry.

Application of physiologically based pharmacokinetic (PBPK) models to predict the biologically effective dose of a compound in the target tissue has gained significant attention in human health risk assessment. The power of PBPK models for extrapolation between species, doses, and exposure routes, as well as to provide a platform to integrate diverse data has driven increased application of the models in risk assessment. These same characteristics

Abbreviations: IVIVE, in vitro to in vivo extrapolation; PBPK, physiologically based pharmacokinetic; PD, pharmacodynamics; PK, pharmacokinetics.

* Corresponding author at: The Hamner Institutes for Health Sciences, 6 Davis Drive, Research Triangle Park, NC 27709-2137, USA. Tel.: +1 919 558 1340; fax: +1 919 558 1300.
E-mail addresses: myoon@thehamner.org (M. Yoon), gkedderis@msn.com (G.L. Kedderis), Zhixia.Yan@fda.hhs.gov (G.Z. Yan), hclewell@thehamner.org (H.J. Clewell III).

http://dx.doi.org/10.1016/j.tox.2014.05.006
0300-483X/

make PBPK modeling a promising tool to bridge between findings from cell-based toxicity/dosimetry experiments and estimates of safe exposure in humans. Further implementation of PBPK models in QIVIVE to support risk assessment, however, has been hampered by the challenges associated with obtaining extensive chemical-specific data to parameterize the model. Reliance on in vivo animal data to estimate parameters and extrapolation of those estimates to a human model has frequently raised the issue of uncertainty in the PBPK model parameters and their propagation to uncertainty in model predictions (Barton et al., 2007).

Remarkable advances in in vitro technologies in recent years open the possibility of incorporating in vitro-derived kinetic parameters directly into PK or PBPK models. To date, such QIVIVE has been performed for only a few environmental chemicals (Kedderis and Held, 1996; Lipscomb and Poet, 2008; Yoon et al., 2012a). In the present study, carbaryl was selected as a case compound for the development of a PBPK model based on the proposed QIVIVE approach. Our previous PBPK/PD model for carbaryl was based on in vivo time-course data from rat studies (Nong et al., 2008). Bayesian uncertainty analysis of this rat model revealed large uncertainties in the carbaryl-specific parameters, including those for metabolism and interactions with cholinesterases (ChEs) (Nong et al., 2008). We started with the rat model because our strategy for building a human model is based on an IVIVE parallelogram approach (Yoon et al., 2012b).

Carbaryl is a widely used insecticide with many agricultural and residential uses. The mode of action for carbaryl toxicity is considered to be carbamylation of, and consequently inhibition of, acethylcholinesterase (AChE) in the peripheral and central nervous systems (Main, 1969; McDaniel et al., 2007; Padilla, 1995; Sogorb and Vilanova, 2002). Inhibition of ChEs by carbaryl is, however, a reversible process (Main, 1969). Since the parent compound is responsible for its anticholinesterase activity, metabolism of carbaryl represents a detoxication process which is mediated by several different forms of CYPs and esterases in the liver (Sogorb and Vilanova, 2002; Tang et al., 2002) as well as esterases in the blood (McCracken et al., 1993; Sogorb and Vilanova, 2002). Recent studies by Herr and colleagues showed that the degree of ChE depression by carbaryl in the brain or red blood cells (RBCs) is a function of carbaryl concentration in the brain or blood (Herr et al., 2010).

In this study, various in vitro data were collected to provide estimates of parameters for carbaryl metabolism, distribution, and its inhibition of ChEs in vivo. The emphasis of this case study was on evaluating the QIVIVE approach and to suggest directions for further studies to refine the approach.

2. Materials and methods

2.1. In vitro studies

2.1.1. Chemicals

Carbaryl (1-naphthyl methylcarbamate, CAS No. 63-25-2) was purchased from Supelco (Bellefonte, PA, USA) and the purity was >99.5%. Collagenase (Type 2, lot# 47A9338) was obtained from Worthington Biochemical Co. (Lakewood, NJ, USA). Williams' Medium E was obtained from Invitrogen (Carlsbad, CA). Radio-labeled carbaryl (98.6%, 1-naphthlenyl methylcarbamate-4a,5,6,7,8,8a-^{14}C6) was kindly provided by Dr. Michael Krolski from Bayer Cropscience Research Park (Stilwell, KS, USA). ^{14}C-labeled carbaryl stock solution was made at 40 mM (300 dpm/0.01 nmol carbaryl) and was diluted appropriately before use. α-Naphthyl-sulfate was obtained from VWR (Radnor, PA). Standards for other carbaryl metabolites were kind gifts from Drs. Michael Krolski and David Herr from the United State Environmental Protection Agency (RTP, NC, USA). They were 3-hydroxycarbaryl, 4-hydroxycarbaryl, 7-hydroxycarbaryl, trans-5,6-dihydro-5,6-dihydroxycarbaryl, and N-hydroxymethyl carbaryl. HPLC grade methanol and 2-propanol were obtained from Sigma–Aldrich (St. Louis, MO, USA). Acethylthiocholine iodide, 6,6′-dithionicotinc acid, tetraisopropylpyrophosphoramide (iso-OMPA), 1-aminobenzotriazole, 1,5-bis(4-allyldimethylammoniumphenyl)pentan-3-one dibromide (BW284c51), and bis-para-nitrophenylphosphate (BNPP) were also obtained from Sigma–Aldrich. All other chemicals were highest grade available from commercial sources.

2.1.2. Animals

Adult male Sprague-Dawley (Crl:CD(SD)) rats between 9 and 12 weeks old (Charles River Laboratories, Raleigh, NC) were housed in the Animal Care Facility of The Hamner Institutes for Health Sciences which is accredited by the Association for Assessment and Accreditation of Laboratory Animal Care International. Rats were acclimated in a temperature- and humidity-controlled, HEPA-filtered environment on a 12 h light–dark cycle. NIH rodent diet (NIH-07, Zeigler Bros., Gardner, PA) and reverse-osmosis water were provided ad libitum. This study was approved by The Hamner Institute's Animal Care and Use Committee.

2.1.3. Rat hepatocytes and other tissue collection

Rat hepatocytes were isolated using a collagenase perfusion method as described in Kedderis et al. (1988). Only hepatocyte preparations of >80% viability determined by trypan blue exclusion were used within an hour after preparation. For collecting blood and tissues, rats were euthanized by CO_2 asphyxiation prior to the necropsy. Blood was collected into heparinized containers and spun down to separate plasma and red blood cells (RBCs). Blood and tissue samples were kept frozen under −80 °C until use.

2.1.4. Procurement of human hepatocytes, plasma and RBCs

Cryopreserved primary human hepatocytes from six individual male donors between the ages of 19 and 48 were purchased from Invitrogen Corporation (Life Technologies, Inc., Durham, NC). Further information on donor demographics can be found in Supplementary material (Table S1). Donor-matched human plasma and washed RBCs were also from six individual male donors between the ages of 18 and 50 (Bioreclamation, LLC, Westbury, NY). Although freshly isolated hepatocytes have been considered as the most superior in vitro model for metabolism studies, cryopreserved hepatocytes have shown comparable metabolic activities to fresh cells indicating their utility in in vitro to in vivo extrapolation (Floby et al., 2009; McGinnity et al., 2004).

Supplementary table related to this article found, in the online version, at http://dx.doi.org/10.1016/j.tox.2014.05.006.

2.1.5. HPLC analysis of carbaryl and its metabolites

HPLC analysis with both UV and radiochemical detection was used for a quantitative analysis of ^{14}C-carbaryl and its metabolites in hepatocyte or plasma incubates. Agilent 1100 HPLC system (Agilent Technologies, Inc, Santa Clara, CA) was used with a C12 Synergi 4 μMAX-RP80A column (250 mm × 4.6 mm, Phenomenex, Torrance, CA). A gradient elution was used using solvent A (20% methanol and 80% of 3.5 mM tetrabuthyl ammonium in water) and solvent B (40% 2-propanol and 60% of methanol) with a flow rate at 1 ml/min and 50 μl of injection volume. The column temperature was kept at 35 °C. UV detection was performed at 210 nm. Radioactivity was quantified using the FSA500TR flow scintillation analyzer with the Flo-One software (PerkinElmer, Inc, Shelton, CT). For UV detection, 1,7-dihydroxynaphthalene was used as an internal standard. Peaks were identified by reference to HPLC retention times of known standards. Chromatograms of all the tested carbaryl metabolites and carbaryl under the current

analytical condition not overlapped each other. Peak areas for carbaryl, 1-naphthol sulfate, and 1-naphthol were used for calculating their respective concentrations in the incubation mixture. For calibration curves, known concentrations of ^{14}C-labeled carbaryl or un-labeled carbaryl and 1-naphthol were used for radioactivity or UV detections, respectively. Although other metabolites of carbaryl including trans-5,6-dihydro-5,6-dihydroxycarbaryl and one of its mono-hydroxylated metabolites were also observed after prolonged incubation of carbaryl with hepatocytes under the current experimental conditions, quantification of those peaks were not performed since they were not necessary for the purpose of study.

2.1.6. Carbaryl metabolism in primary hepatocytes and plasma

2.1.6.1. Hepatocytes. The freshly isolated hepatocytes (0.25×10^6 or 0.083×10^6 cells/ml) were suspended in 3 ml of Williams' Medium E, in sealed Erlenmeyer flasks containing 5% CO_2 in air (to maintain pH) and incubated with various initial concentrations of ^{14}C-carbaryl or 1-naphthol, respectively, at 37 °C in a Dubnoff shaking incubator (60 cpm). Final concentration of methanol did not exceed 0.2% in the incubation mixture. The reaction was terminated at predetermined time points by adding 2 ml of 0.6% (v/v) formic acid in methanol. Samples were centrifuged and the supernatant was used for HPLC analysis immediately after preparation. The assay was performed in duplicates. Time-dependent disappearance of carbaryl and formation of 1-naphthol-sulfate were determined based on readioactivity signal, while those of 1-naphthol and formation of sulfate conjugate of 1-naphthol were determined based on UV absroption.

Cryopreserved human hepatocytes were thawed quickly at 37 °C in a water bath, and transferred into pre-warmed William's medium E. After centrifugation at room temperature at $100 \times g$ for 10 min, the cells were re-suspended in William's medium E before determining cell numbers and viability by trypan blue exclusion. Hepatocytes suspensions (0.4×10^6 cells/ml) were then pre-incubated with or without 1-aminobenzotriazole (1-ABT, 1 mM) at 37 °C with gentle shaking for 30 min before adding carbaryl into the cell suspension. The final concentrations of carbaryl in the reaction mixture were either at 5 or 50 μM in a total volume of 1 ml. The reaction was terminated by adding 0.66 ml of 0.6% (v/v) formic acid in methanol after 30, 60 and 90 min after incubation. Samples were immediately processed for HPLC analysis as described for the rat hepatocyte assays. Time-dependent disappearance of carbaryl was measured by HPLC with UV detection at 210 nm.

2.1.6.2. Plasma. Rat or human plasma was incubated in 0.1 M phosphate buffer (pH 7.4) at 37 °C with gentle shaking (60 cpm) with final concentration of carbaryl at 10 or 75 μM for rat and 5 μM for human plasma in 0.5 ml total incubation volume. The final concentration of vehicle (methanol) was less than 0.2%. To determine the extent of contribution of butyrylcholinesterase or Ca^{2+}-dependent esterase(s) to the hydrolysis of carbaryl in plasma, human plasma was preincubated with iso-OMPA (0.1 mM) or EDTA (6 mM), respectively, for 5 min before adding carbaryl into the incubation mixture. The incubation was stopped at predetermined time points by adding 0.33 ml of 1.6% of formic acid in methanol. The assays were conducted in duplicate. The incubates were centrifuged and the supernatant was immediately used for HPLC analysis. 1-Naphthol was the only metabolite detected in plasma after incubation with carbaryl under the current assay conditions. Disappearance of carbaryl and appearance of 1-naphthol (in the case of rat plasma only) as a function of incubaton time was determined using HPLC with UV detection as described above.

2.1.6.3. Chemical hydrolysis. Spontaneous hydrolysis of carbaryl at physiological pH (7.4) and temperature (37 °C) was determined at three different concentrations of carbaryl (final concentrations of 10, 40, and 75 μM) using the same assay conditions used for the plasma metabolism studies. Formation of 1-naphthol after incubation of carbaryl in 0.1 M phosphate buffer for upto 60 min was determined and a first order rate constant (min^{-1}) for carbaryl degradation by chemical hydrolysis was calculated (GraphPad Prism 4.0, GraphPad Software, La Jolla, CA).

2.1.7. Determination of unbound fraction of carbaryl in the blood and tissue homogenates

2.1.7.1. Equilibrium dialysis. The unbound fraction (fu) of carbaryl in plasma, RBCs and various tissue homogenates was determined using a rapid equilibrium dialysis (RED) method (Yan et al., 2011). Tissue homogenates of brain, liver, fat, muscle and plasma, RBCs, and whole blood were used for SD rats, whereas plasma and RBCs were used for humans. RED was conducted as recommended by the manufacturer (Pierce Biotechnology, ThermoFisher Scientific, Waltham, MA) with slight modifications. In our assay, ^{14}C-labeled carbaryl in 0.01 M PBS (20 μM) was loaded in the buffer chamber, whereas each tissue homogenate in 0.01 M PBS was loaded into the sample chamber. The RED plate was incubated for 4 h on a thermomixer (Eppendorf AG, Hamburg, Germany) at 37 °C with vigorous and continuous vortexing at 500 rpm. The assay was performed in triplicates. Preliminary results using the rat samples showed that 4 h incubation was sufficient to reach equilibrium between the two chambers. To determine fu in hepatocytes suspensions, Williams' Medium E was used instead of PBS.

The fu in a given tissue was defined as a ratio of total carbaryl concentration in the buffer chamber to that in the sample chamber at the end of incubation. The tissue or plasma to PBS partition coefficient ($PC_{t:PBS}$ or $PC_{p:PBS}$, respectively) for carbaryl was the ratio of the concentration of total carbaryl in the given tissue to the concentration of total carbaryl in the PBS, which is the same as the reciprocal of fu in the given tissue or plasma. The tissue to plasma partition coefficient ($PC_{t:p}$) was calculated based on the ratio of $PC_{t:PBS}$ to $PC_{p:PBS}$ (Table 3). The fu values determined from diluted tissue samples were corrected to obtain an estimate of the corresponding, true fu in the undiluted tissue according to Kalvass and Maurer (2002). The undiluted fu was calculated as $(1/D)/[((1/fu2) - 1) + 1/D]$, where D represents a dilution factor, whereas fu2 is the unbound fraction measured following a known fold dilution of the given tissue.

2.1.8. Interaction of carbaryl with cholinesterases

2.1.8.1. Enzyme activity assay. Fresh RBCs were used for the assay, while plasma and brain homogenates were kept frozen until the assay. The activity of AChE or BuChE in diluted tissue samples was determined based on the modified Ellman method (Ellman et al., 1961; Nostrandt et al., 1993). The assays were conducted in a 96-well plate using a temperature controlled-microplate spectrophotometer (SpectraMax 340, Molecular Device, Inc, Sunnyvale, CA). The assay was run in duplicate using acethylthiocholine (ATC, 0.1 mM) as a substrate both for AChE and BuChE and 6,6′-dithhionicotinic acid (DTNA, 0.4 mM) as a dithiol agent (Kousba et al., 2007). Changes in absorbance at 340 nm were monitored for 10 min at 37 °C. ChE activity (μmol/min/ml sample) was calculated using the slope of the linear portion of this time-course curve (mOD/min) with a molar extinction coefficient of DTNA chromophore (10^4 M^{-1} cm^{-1}) (Brownson and Watts, 1973). Appropriate blank rates were subtracted to correct for non-enzyme mediated hydrolysis of ATC and for potential interference of absorbance by hemoglobin in the case of RBCs.

For plasma, all the incubations and measurements were performed in the presence of EDTA and BNPP at final concentrations of 6 mM and 0.1 mM, respectively, to minimize potential hydrolysis of carbaryl by Ca^{+2} dependent A-esterase and carboxylesterases

present in plasma (McCracken et al., 1993; Tang and Chambers, 1999). Plasma AChE activity was measured in the presence of 0.1 M iso-OMPA to inhibit BuChE activity, while plasma BuChE activity was determined with 0.01 M BW284C51 to inhibit AChE activity (Kousba et al., 2003; Maxwell et al., 1987). For the brain and RBCs, only AChE activity was determined as it is the predominant ChE in the brain and the only ChE in RBCs. For humans, plasma BuchE and RBC AchE activities were similarly determined, while plasma AChE activity was not determined as it is not present in human plasma.

2.1.8.2. Determination of inhibition and regeneration of ChE activities. Carbaryl-induced inhibition of and subsequent recovery of the enzyme activities were determined based on Kousba et al. (2007) and Groner et al. (2007) with slight modifications. To determine the inhibition of AChEs by carbaryl, brain homogenate or RBCs from rats was diluted and incubated in 0.01 M PBS containing various concentrations of carbaryl for different duration of time for up to 7 min in a thermomixer (Eppendorf AG, Hamburg, Germany) with gentle shaking. The inhibition was stopped by adding a large volume of 0.01 M PBS containing ATC and DTNA at final concentrations of 0.4 and 0.1 mM, respectively, immediately after which AChE activity was determined in each sample as described above. Rat plasma AChE and BuChE activities were similarly measured except that the diluted plasma samples were pre-incubated for 5 min with either iso-OMPA or BW284C51 prior to adding carbaryl to the incubate. To determine the rate of recovery of enzyme activity, samples were first incubated with carbaryl for 5 min to inhibit enzymes. The inhibition was stopped by adding a large volume of 0.01 M PBS and followed by further incubation for various durations up to 45 min to allow decarbamylation of the carbamylated enzymes. All incubations were performed at 37 °C.

2.1.8.3. ChE inhibitory and recovery rate constants. The bimolecular inhibition rate constant (k_i, $\mu M^{-1}\ h^{-1}$) was calculated based on Main's approach (Main, 1969). The natural log values of % remaining ChE activity were plotted as a function of the duration of inhibition at each carbaryl concentration. The slopes of the linear portion of each of these semi-log plots were calculated using a linear regression analysis, the reciprocals of which were then plotted against 1/[carbaryl]. The slope from the resulting double reciprocal plot for each animal was used to calculate k_i for the given tissue in each individual rat. The rate constant for decarbamylation, i.e., the first order rate constant for recovery of the enzyme activity (k_r), was calculated by fitting the % remaining activity versus time after cessation of inhibition to a single exponential curve assuming the control activity (the uninhibited activity) as the activity of the fully recovered enzyme using the GraphPad Prism (GraphPad Software Inc. La Jolla, CA).

2.2. Extrapolation of in vitro-derived parameters

2.2.1. In vitro kinetic modeling

A PK model was used to describe carbaryl metabolism in hepatocytes or plasma as shown in Fig. 1. In vitro metabolic constants were estimated using the automated parameter estimation function in acslX (The AEgis Technologies Group, Inc., Huntsville, Alabama) by fitting this in vitro model to the time course data from hepatocytes or plasma incubations. The average of all the individual observations at each time point was used for this purpose.

2.2.2. Consideration of free concentration in vitro

In this study, only free (unbound) carbaryl was assumed to be available for metabolism in hepatocytes and thus, in the liver. The experimentally measured fu in the hepatocyte incubation mixture was incorporated in the in vitro PK model. This was applied only to the rat hepatocytes, as most of the carbaryl was found to be unbound (fu = 0.88) in the hepatocyte incubation system. Therefore, all the carbaryl was assumed to be unbound for human hepatocyte modeling. As the plasma was diluted 25-fold with phosphate buffer for the assay, all the carbaryl in the plasma incubation mixture was assumed to be free.

A mass-balance study performed with ^{14}C-labeled carbaryl in the incubation mixture with hepatocytes suspension or plasma indicated no significant non-specific binding of carbaryl to tissue/cell components or assay vessels, i.e., less than 1% of total radioactivity, during incubation. Therefore, no adjustment was made to account for non-reversible binding or non-specific binding of carbaryl in hepatocyte suspensions or in plasma.

2.2.3. In vitro to in vivo extrapolation of metabolic constants

Biologically relevant scaling methods were used as described by Kedderis (2007). The metabolic capacity (V_{max}) or clearance (CL_{int}) was scaled based on the total enzyme content in the in vitro assay system (e.g., hepatocytes) compared to the respective metabolic site in vivo (e.g., liver), while the affinity constant (K_m) was directly used in the model without scaling (Table 1). The scaling factor used for hepatocytes experiment-derived metabolic constants was hepatocellularity, for which 117 and 99 million cells/g liver were used for rats and humans, respectively (Barter et al., 2007; Sohlenius-Sternbeck, 2006). Plasma CL_{int} was scaled up on the basis of volume of plasma.

2.3. PBPK modeling of carbaryl kinetics

2.3.1. Model structure

The previously published rat PBPK model for carbaryl (Nong et al., 2008) was revised to incorporate in vitro data collected in this study (Fig. 6). The model simulates two different routes of carbaryl exposure, one by oral ingestion and the other by intravenous (IV) injection. All the tissues were described as diffusion-limited, although the tissue permeability-area product for liver makes this tissue essentially a flow limited compartment (Table 1). Blood was divided to plasma and RBCs. Exchange of carbaryl between plasma and RBCs was assumed to be rapid. The ratio between the two is governed by RBCs:plasma partition coefficient (Table 3). Protein binding kinetics in plasma was assumed to be rapidly reversible and would not limit diffusion of carbaryl across tissue cellular membranes while the blood (plasma) passes through the tissue.

In the current model, elimination of carbaryl occurs only by metabolism. Compared to the previous model, description for metabolism was simplified as our purpose was to evaluate IVIVE approach for active form of carbaryl, which was the parent form, not to fully describe kinetics of all the metabolites of carbaryl. To this end, degradation of carbaryl by CYP-mediated metabolism was regarded as elimination from the body. Metabolism of carbaryl was assumed to occur only in the liver and plasma, for which the same description was used as in vitro PK models for hepatocytes and plasma incubation systems (Fig. 1). It should be noted that the experimentally measured fu values were used in describing the substrate (carbaryl) availability in each metabolic site, in the liver and plasma.

For kinetics of 1-naphthol formed from carbaryl, we used a one-compartment model like approach (Fig. 6). The plasma to tissue partition coefficient of 1-naphthol was all set to 0.7 for brain, fat, and rest of body assuming the distribution of this metabolite to total body water. As it was expected to be a major metabolite of 1-naphthol in the liver, a separate one compartment model for 1-naphthol sulfate was described (Fig. 6). The volume of distribution for 1-naphthol sulfate was assumed to be 0.25 L/kg based on the observation that 1-naphthol sulfate was only detected in plasma (Nong et al., 2008). Urinary excretion of 1-naphthol sulfate was described using a first order rate constant. A first order rate constant

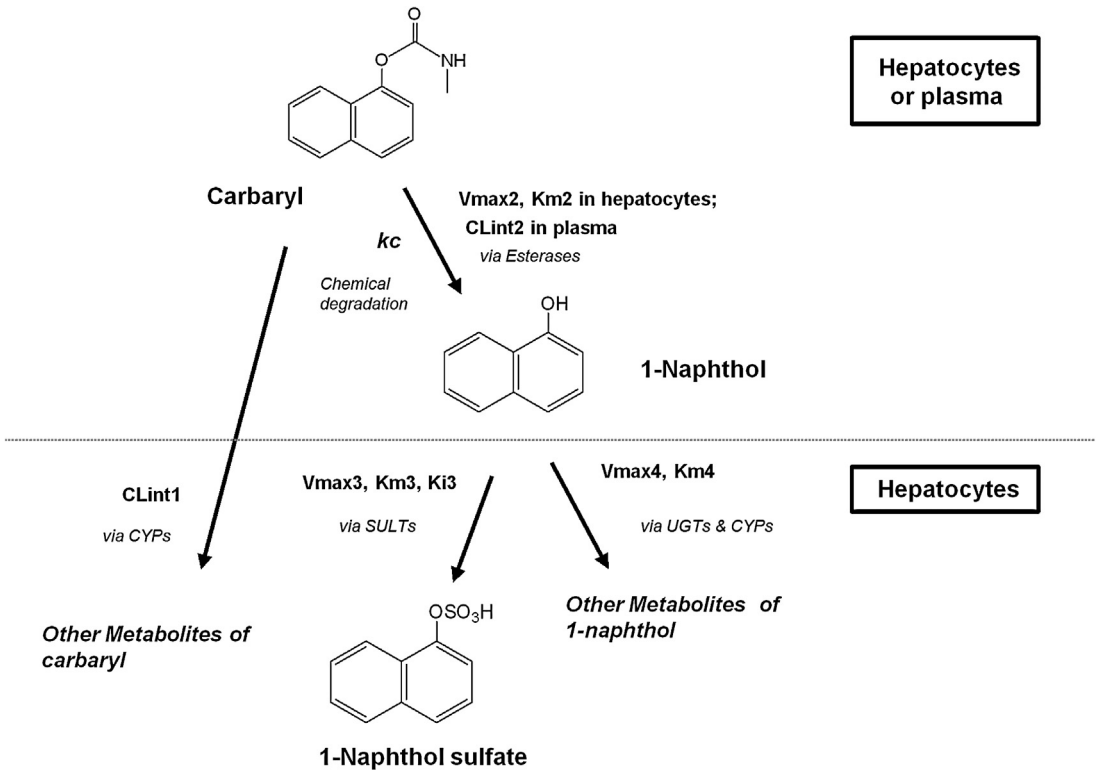

Fig. 1. In vitro PK model to describe carbaryl metabolism in hepatocytes or plasma CL_{int1} corresponds to CL_{rat1} or CL_{human1} for rat or human hepatocytes, respectively, whereas CL_{int2} corresponds to CL_{rat2} or CL_{human2} for rat or human plasma, respectively. For rat hepatocytes, UGTs and SULTs represent UDP-glucuronosyltransferases and sulfotransferases, respectively. Refer to Table 1 for other abbreviations used in the scheme.

Table 1
Scaling of in vitro carbaryl metabolism parameters for in vitro to in vivo extrapolation.

	In vitro		In vivo		Description
	Value	Unit	Value	Unit	
SD rat					
CL_{rat1}	0.022	ml/min/10^6 cells	156	L/h/kg liver	Clearance of carbaryl via formation of metabolites other than 1-naphthol in the rat liver/hepatocytes
V_{max_2}	0.312	nmol/min/10^6 cells	2190	μmol/h/kg liver	Maximum rate of carbaryl metabolism to 1-naphthol, in the rat liver/hepatocyte, enzymic
KM2	34.0	μM	34	μM	Michaelis–Menten constant for 1-naphthol formation in the rat liver/hepatocyte
V_{max_3}	1.02	nmol/min/10^6 cells	7160	μmol/h/kg liver	Maximum rate of 1-naphthol metabolism to its sulfate conjugate in the rat liver/hepatocyte
KM3	0.076	μM	0.076	μM	Michaelis–Menten constant for 1-naphthol sulfate formation in the rat liver/hepatocyte
k_{i_3}	31.0	μM	31	μM	Substrate inhibition constant for1-naphthol sulfate formation in the rat liver/hepatocyte
V_{max_4}	3.30	nmol/min/10^6 cells	23,194	μmol/h/kg liver	Rate of 1-naphthol metabolism other than sulfation in the rat liver/hepatocyte
KM4	17.0	μM	17	μM	Michaelis–Menten constant for 1-naphthol metabolism other than sulfation in the rat liver/hepatocyte
CL_{rat2}	0.060	ml/min/ml plasma	3.6	L/h/kg plasma	Clearance of carbaryl via hydrolysis to 1-naphthol in the rat plasma, enzymic
Human					
CL_{human1}	0.004	ml/min/10^6 cells	22	L/h/kg liver	Clearance of carbaryl via metabolism in the human liver/hepatocyte, total enzymic
CL_{human2}	0.395	ml/min/ml plasma	24	L/h/kg plasma	Clearance of carbaryl via hydrolysis to 1-naphthol in the human plasma, enzymic
Chemical					
k_C	0.00071	/min	0.043	/h	Rate of spontaneous hydrolysis of carbaryl at physiological pH and temperature, chemical

Note: Metabolic constants for rats and humans were estimated using acslX parameter estimation function using the carbaryl and metabolites concentration data from multiple independent experiments performed with tissues from each individual donor. Hepatocellularity for in vitro to in vivo scaling was 117 and 99 million cells/g liver for rats and humans, respectively (Barter et al., 2007; Sohlenius-Sternbeck, 2006).

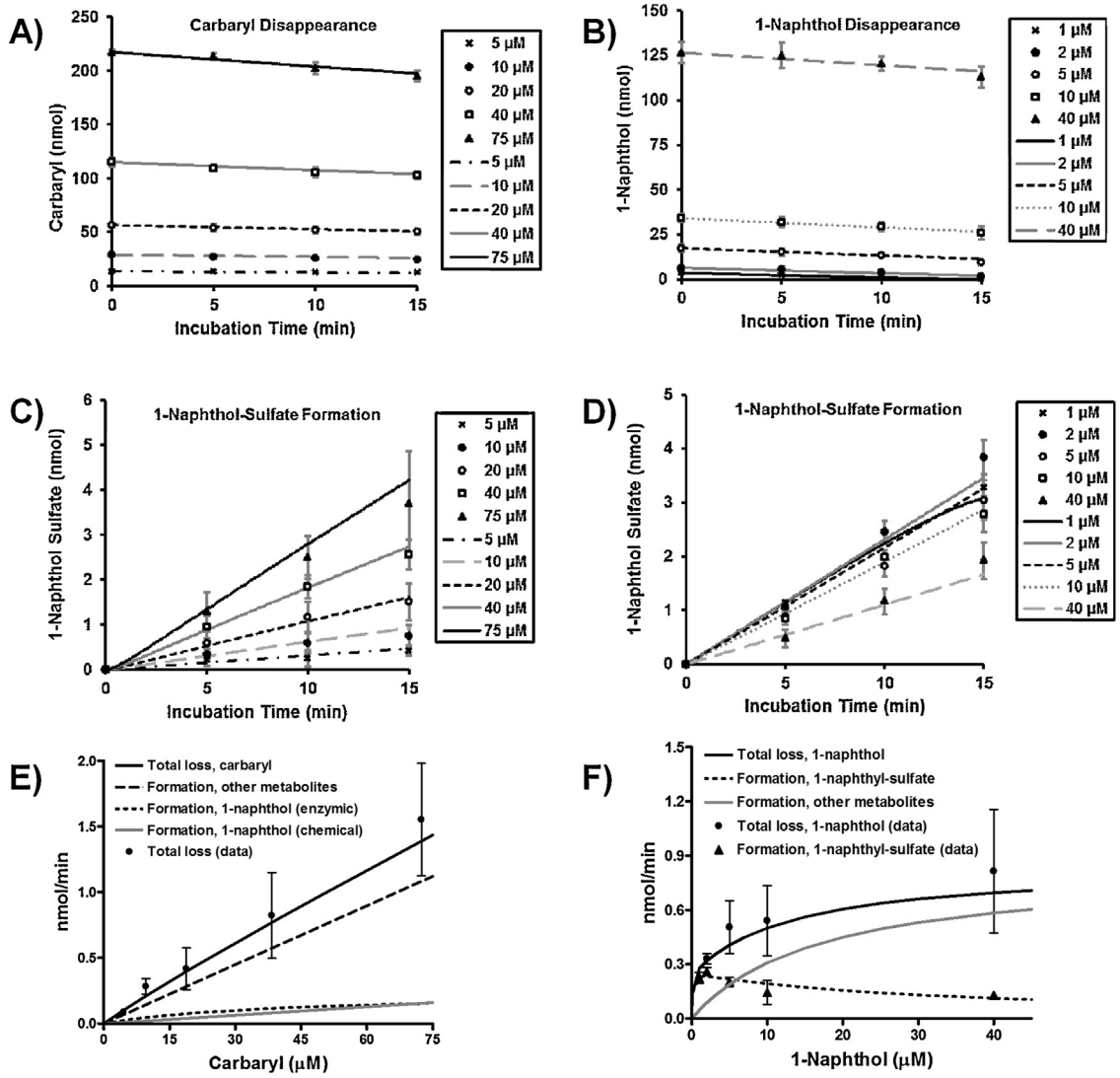

Fig. 2. Determination of metabolism of carbaryl and its metabolite 1-naphthol in SD rat hepatocytes. Symbols represent the mean ± SD calculated from 3 or 4 individual animal experiments. Lines represent model simulations using the parameter values obtained from fitting the in vitro model to the time course data both from carbaryl and 1-naphthol incubation studies.

for urinary excretion of total 1-naphthol in humans, the majority of which was conjugate(s) of 1-naphthol, was first estimated (Holm et al., 2013; Yoon et al., 2012b). The respective rat value was estimated using GFR ratio approach as was done by Yan et al. (2012) and used as a first order rate constant for 1-naphthol sulfate urinary excretion in this model. No urinary excretion of free 1-naphthol was included in the model. Other metabolite(s) of 1-naphthol were treated as elimination from the body.

During this modeling, we found that further elaboration on carbaryl absorption and potential intestinal metabolism of this compound in the gut would be necessary to improve model performance for oral exposure (Fig. 7). The absorption of carbaryl was a first order process with a high absorption rate constant, k_a (Hwang and Schanker, 1974). Only a fraction of the dose is absorbed (FA) from the gut lumen to intestinal epithelial cells. Then, a fraction (FM) of this absorbed carbaryl is metabolized within enterocytes before reaching to systemic circulation further reducing oral bioavailability. The FA and FM values were estimated to let the model outputs be consistent with the observed time-courses for carbaryl in the brain and 1-naphthol sulfate in the plasma following a single oral gavage at 8.45 mg/kg (Nong et al., 2008).

Binding of carbaryl to active sites in ChEs and subsequent decarbamylation of them were described for brain, plasma, and RBCs for the respective ChE(s) present in each tissue. Only free (unbound) carbaryl binds to ChEs in the model. Experimentally determined fu values for brain, RBCs, and plasma (Table 3) were used for this purpose. Binding of carbaryl to and resulting inhibition of ChEs was described with k_i, a bimolecular reaction rate constant. Binding occurred between the free ChE enzyme and carbaryl. The regeneration of enzyme activity resulted from decarbamylation of carbaryl-bound ChE, for which a first order rate constant, k_r, was used. Carbaryl concentration in each tissue that interacts with ChEs was provided from the PBPK part of the model. Rates of synthesis and degradation for each type of ChEs were included in the model along with their basal expression levels (Table 1).

2.3.2. Model parameterization

All the physiological and chemical specific parameters other than those in vitro-derived (Tables 1 and 4) were taken from the previously published rat model (Nong et al., 2008). The in vitro-based parameters were metabolic parameters for carbaryl and 1-naphthol in the liver and plasma; and binding and liberation of carbaryl to and from ChEs in the brain, red blood cells (RBCs), and

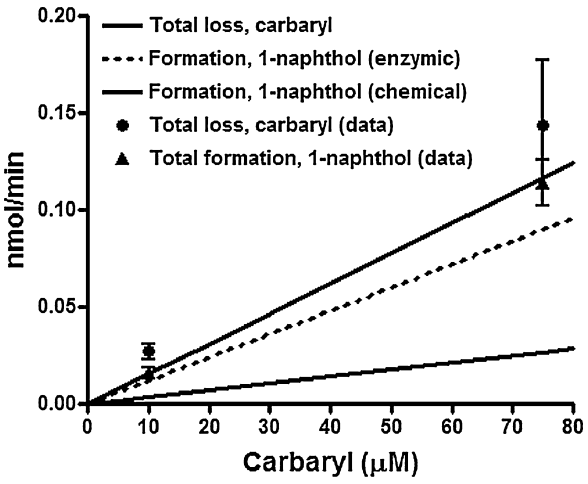

Fig. 3. Determination of carbaryl metabolism in SD rat plasma. Symbols represent the mean ± SD calculated from 4 individual animal experiments. Lines represent model simulations using the parameter values obtained from fitting the in vitro model to the time course data. Preliminary experiments showed that carbaryl degradation in SD rat plasma was linear up to 75 μM initial concentration of carbaryl. 1-Naphthol was the only metabolite in in vitro plasma incubation studies.

plasma. They were scaled up to in vivo as described in Section 2.2.3. For some parameters, a few alternative strategies for IVIVE were explored before incorporation in the model as detailed in Section 3.

2.3.3. Sensitivity analysis

A sensitivity analysis was conducted as described in Yoon et al. (2009). The relative influence of each of the model parameters on simulated brain carbaryl concentration 40 min after the dosing, either oral or IV, was examined based on the calculated sensitivity coefficient (SC) values. All the model parameters were subject to the sensitivity analysis and those with SC greater than 0.2 for the dose metrics from either dosing studies were reported (Table 5).

2.3.4. Model simulations

All the model simulations were run using acslX (version 3.0.2.1; The Aegis Technologies Group, Inc., Huntsville, Alabama).

3. Results

3.1. In vitro pharmacokinetic studies

3.1.1. Determination of carbaryl metabolism parameters in rats

3.1.1.1. Rat hepatocytes. Under the current experimental conditions, the rate of degradation of carbaryl in SD rat hepatocytes was linear and no saturation was observed over the range of substrate concentrations (Fig. 2A and C). The maximum substrate concentration in this study was limited to 75 μM due to solubility. 1-Naphthyl sulfate, but not free 1-naphthol, was detected after the incubation of hepatocytes with carbaryl, suggesting a rapid and complete conversion of 1-naphthol to its conjugate(s), mainly to the sulfate conjugate at the initial carbaryl concentrations used. When incubated with hepatocytes, disappearance of 1-naphthol was linear over the range of substrate concentration used in this study (Fig. 2B). However, formation of 1-naphthyl sulfate was not linear at higher substrate concentrations suggesting atypical or non-Michaelis–Menten kinetics (Fig. 2D).

3.1.1.2. Rat plasma. Hydrolysis of carbaryl in RBCs appeared to be negligible since the carbaryl concentration did not change after incubation with RBCs under the current experimental conditions (data not shown). 1-Naphthol was the only metabolite detected when carbaryl was incubated with rat plasma. The rate of carbaryl disappearance and hence the formation of 1-naphthol in plasma was linear under the experimental conditions used for both initial substrate concentrations of 10 μM and 75 μM of carbaryl (Fig. 3). Therefore, the intrinsic clearance (CL_{int}) of carbaryl degradation in rat plasma (CLrat2) was estimated with both datasets using an in vitro PK model (Table 1).

3.1.2. Determination of carbaryl metabolism parameters in human hepatocytes and plasma

3.1.2.1. Human hepatocytes. When incubated with carbaryl, 1-naphthol and its conjugates were not detected in human hepatocytes at low carbaryl concentration. Either or both were observed only in a few cases at high concentration of carbaryl. Based on these findings, CYPs-mediated oxidation was considered to be a major metabolic pathway for carbaryl in human hepatocytes as in the rat. Based on rat hepatocyte results in which linear metabolism of carbaryl was observed, an CL_{int} (CL_{human1}) was used to describe total carbaryl degradation in human hepatocytes instead of using the apparent V_{max} and K_m explicitly (Fig. 4). Our results support a conclusion that the deviation from linearity in carbaryl metabolism would not be significant for up to 50 μM as indicated by similar average values of CL_{int} between 5 and 50 μM carbaryl initial concentrations (Fig. 4A). The CL_{int} of carbaryl in human hepatocytes was estimated using the data with 5 μM carbaryl only (Table 1).

Pretreatment with 1-aminobenzotriazole (1-ABT), a non-selective mechanism-based inhibitor of CYP enzymes, had no significant impact on carbaryl CL_{int} at 5 μM, while metabolism

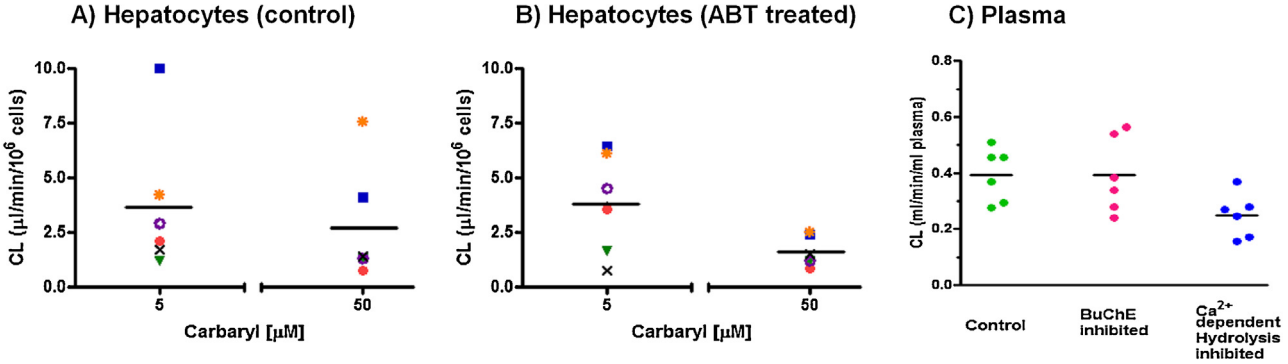

Fig. 4. Determination of carbaryl clearance in human hepatocytes and plasma. Each symbol represents the CL_{int} determined in hepatocytes (A and B) or plasma (C) from 6 individual donors. In panels (A) and (B), black solid lines indicate the mean of CL values from 6 individual donors at the given carbaryl concentration. CL was measured either in control cells (A) or CYPs-inhibited cells with 1-ABT pretreatment (B). Each symbol represents the CL determined in 6 individual donors at 5 μM carbaryl concentration. EDTA or iso-OMPA was used to specifically inhibit Ca^{2+}-dependent esterases or BuChE activity, respectively (C).

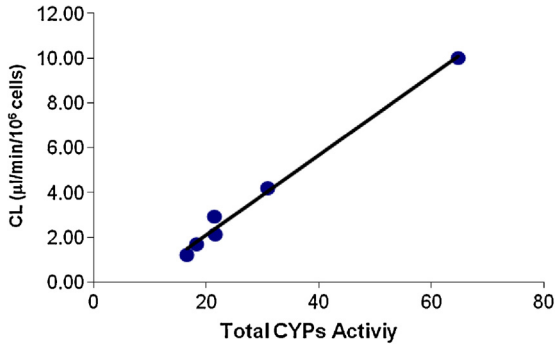

Fig. 5. Correlation of carbaryl clearance at low concentration with total CYPs activity in human hepatocytes. Each symbol represents the CL determined in 6 individual donors at 5 μM carbaryl concentration. ECOD activity (7-ethoxycoumarin-O-deethylation) was used as a marker for general phase I metabolism (total CYPs activity).

was greatly reduced at 50 μM (Fig. 4B). This result suggests the involvement of multiple CYP isoforms in carbaryl metabolism as previously demonstrated with human microsomes and recombinant CYP isoforms (Tang et al., 2002). The CL_{int} at 5 μM correlated well with 7-ethoxycoumarin-O-deethylation (ECOD) activity (Fig. 5), while no apparent correlation was observed at 50 μM carbaryl indicating concentration-dependent changes in the relative contribution of individual isoforms. This observation further supports the involvement of multiple CYPs. ECOD activity in human hepatocytes from each individual donor was provided by the vendor (Life Technologies Co., Durham, NC) as a marker of general phase I metabolism, as its metabolism involves multiple human CYP isoforms (Shimada et al., 1999; Waxman et al., 1991).

3.1.2.2. Human plasma. Hydrolysis of carbaryl to 1-naphthol in human plasma was observed to be linear in the preliminary experiment using 5 and 50 μM carbaryl concentrations (data not shown), as was also observed in rat plasma. The CL_{int} for hydrolysis of carbaryl to 1-naphthol in human plasma (CL_{human2}) was then estimated for a carbaryl concentration of 5 μM (Fig. 4C). The CL_{human2} was greater than that for rats (CL_{rat2}) (Table 1). No significant change was observed in carbaryl hydrolysis in human plasma in the presence of ISO-OMPA; whereas, a significant decrease (by 38% in average) was observed with EDTA, indicating the involvement of Ca^{2+} dependent esterase(s), but not butyrylcholinesterases or carboxylesterases in carbaryl hydrolysis (Fig. 4C).

3.1.3. In vitro kinetic modeling

3.1.3.1. Chemical hydrolysis. Carbaryl was shown to be spontaneously hydrolyzed to 1-naphthol at physiological temperature and pH. A first order rate constant for this hydrolysis was 0.00071 min^{-1}. The observed kinetics for carbaryl disappearance and 1-naphthol sulfate formation in vitro should be interpreted with caution, since the sources of 1-naphthol were from both chemical and enzyme mediated reactions, for which the in vitro to in vivo scaling differs (volume versus enzyme content). Therefore, chemical degradation of carbaryl was accounted for in both in vitro PK and in vivo PBPK modeling.

3.1.3.2. In vitro PK modeling of hepatocyte incubation system. To simulate carbaryl kinetics in rat hepatocytes, two metabolic pathways for carbaryl were described, hydrolysis and oxidative metabolism, both of which are mediated by multiple enzymes (Fig. 1). Our data on the time-dependent disappearance of carbaryl and formation of 1-naphthol sulfate was best described by a first order reaction for oxidative metabolism and a saturable process for enzyme-mediated hydrolysis (Fig. 2A, C and E). The rate of chemical hydrolysis of carbaryl at physiological pH and temperature was taken into account to obtain true enzyme-catalyzed reaction rates for carbaryl degradation.

Table 2
Experimentally determined parameters for carbaryl interactions with ChEs.

Rate constant		Bimolecular inhibition, k_i (/μM/h)	Decarbamylation, k_r (/h)
Rat	Brain AChE	5.14 ± 1.21	2.09 ± 0.46
	RBC AChE	2.67 ± 0.56	1.54 ± 0.41
	Plasma AChE	11.11 ± 1.37	1.60 ± 0.40
	Plasma BuChE	0.53 ± 0.22	0.45 ± 0.10
Human	RBC AChE	3.71 ± 1.56	2.01 ± 0.55
	Plasma BuChE	0.20 ± 0.22	1.19 ± 0.21

Note: Each value represents the mean ± SD for 5 or 6 individuals for rats or humans, respectively.

1-Naphthol in rat hepatocyte suspensions was described by two metabolic fates, one to form the sulfate conjugate and the other to form all other metabolites (Fig. 1). The sulfation showed non-Michaelis–Menten (M–M) kinetics and was described using substrate inhibition kinetics as follows:

$$V = \frac{V_{max_3} \times C_{1\text{-napthol}}}{K_{m_3} + C_{1\text{-napthol}} \times (1 + (C_{1\text{-napthol}}/K_{i_3}))}$$

where V is the rate of sulfation; V_{max_3} is the maximum rate of sulfation; K_{m_3} is the Michaelis–Menten constant; and k_{i_3} is the inhibitory constant for substrate binding (Copeland, 2002). The pathway for other metabolites was described using the typical M–M equation with apparent V_{max_4} and K_{m_4}. Our data and simulations suggested that metabolism of 1-naphthol would be rapid enough to assume that essentially all of the 1-naphthol would be converted to 1-naphthol sulfate within the range of carbaryl concentrations used in this study (Fig. 2E and F).

3.1.3.3. In vitro PK modeling of plasma incubation system. CL_{int} values in rat plasma obtained from the two assays with different initial concentrations (10 and 75 μM) were similar, so they were averaged to obtain CL_{rat2} (Table 1). CL_{human2} in vitro was similarly estimated using the data with 5 μM initial substrate concentration.

3.2. In vitro cholinesterase inhibition studies

3.2.1. Determination of parameters for carbaryl interaction with ChEs

The k_i values from brain AChE, RBC AChE, plasma AChE, and plasma BuChE in SD rats varied depending on the tissue and type of ChE, while k_r values seemed to be consistent for the same type of ChE regardless of species (Table 2).

3.3. IVIVE

3.3.1. Tissue partitioning and free concentration

Partition coefficients were calculated using the in vitro measured fu values as described in Section 2. They are compared to in vivo data-based estimates, as well as to the QSAR predicted values, in Table 3. The unbound fraction in plasma (fup) predicted from the QSAR method (0.21) was close to the experimental result for human (0.16) and rat (0.20). Greater discrepancies were found for brain and fat partition estimates from different methods. In vitro binding data appeared to underestimate both brain- and fat-to-plasma PCs (0.50 and 0.93 vs. 1.0 and 6.0, respectively, in vivo). The QSAR based fat PC was underestimated (3.26 vs. 6.0), whereas it was overestimated for brain (3.42 vs. 1.0) when compared to the corresponding in vivo estimates (Table 3). Therefore, PCs for brain

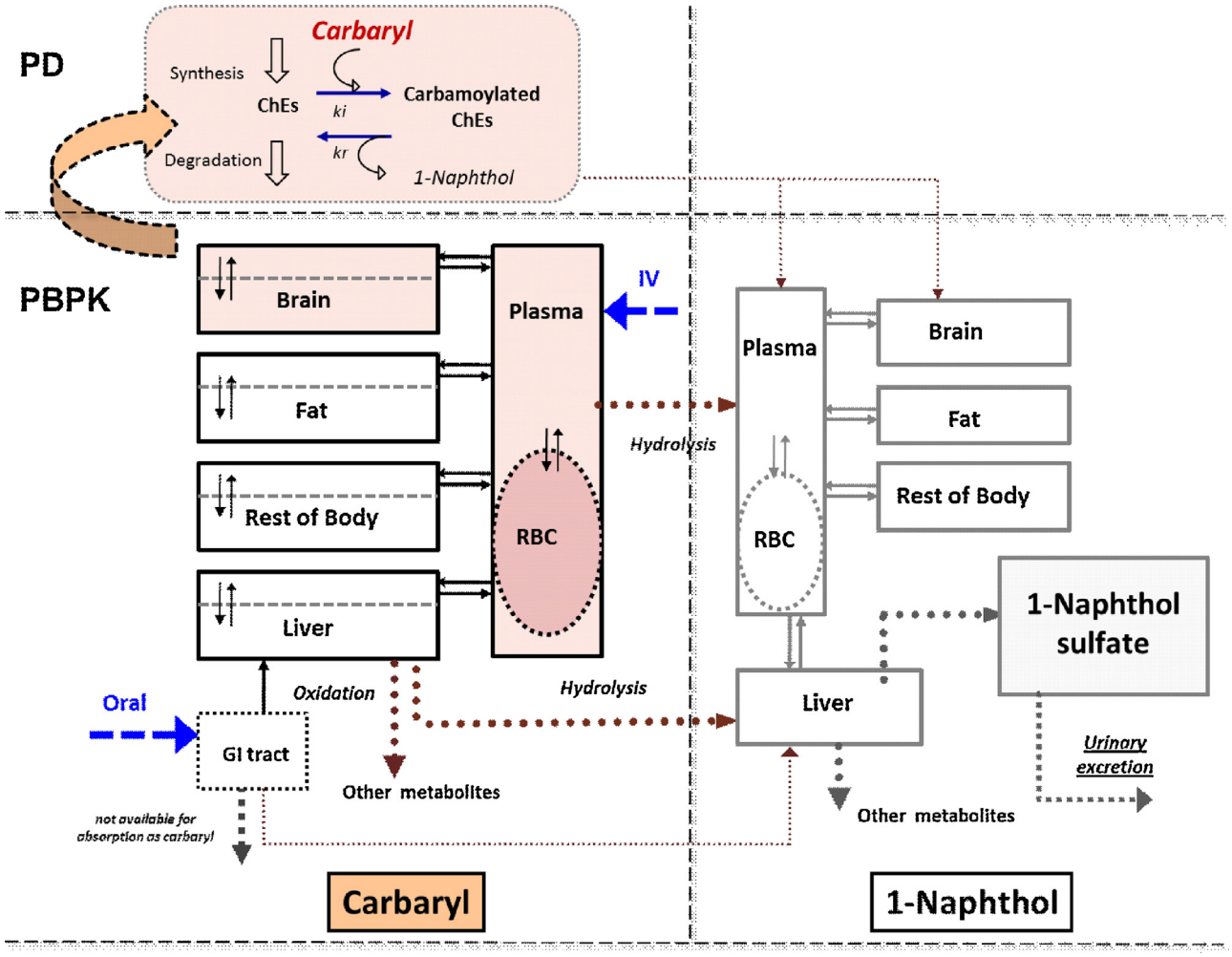

Fig. 6. Structure of the carbaryl PBPK/PD model.

and fat were taken from the previous model (Nong et al., 2008) in this study (Table 4).

3.3.2. Extrapolation of in vitro-derived biochemical constants

3.3.2.1. Biological scaling of metabolic constants. The parameters for carbaryl metabolism in hepatocytes and plasma were estimated by in vitro kinetic modeling. The description of metabolic processes in the liver and plasma in the PBPK model was the same as in the in vitro model (Fig. 1). The in vitro parameters were extrapolated to the corresponding in vivo counterparts after appropriate conversion so that they could be directly incorporated in the model (Table 1).

Table 3
Tissue to plasma partition coefficient (PC) for carbaryl in selected Sprague Dawley rat and human tissues.

Tissue		fu in tissue homogenate	$PC_{tissue:plasma}$		
			In vitro fu data based	QSAR predicted	
				With Fup = 0.2	With Fup = 0.16
Rat	Whole blood	0.27 ± 0.013	na	na	na
	Plasma	0.20 ± 0.007	na	na	na
	RBC	0.25 ± 0.021	0.78 ± 0.06	na	na
	Brain	0.39 ± 0.038	0.50 ± 0.06	3.42	2.65
	Liver	0.17 ± 0.009	1.15 ± 0.05	1.74	1.36
	Fat	0.23 ± 0.065	0.93 ± 0.30	3.26	2.54
	Muscle	0.31 ± 0.084	0.66 ± 0.14	1.55	1.25
Human	Plasma	0.16 ± 0.005	na	na	na
	RBC	0.27 ± 0.090	0.65 ± 0.16	na	na

Values represent the mean ± SD for 5 or 6 individual rats or human donors, respectively. QSAR predicted $PC_{tissue:plasma}$ were calculated using SimCyp V12. Input for B:P ratio was provided from our data (fup/fub) using the fu values determined in the rat blood and plasma, where fu_b is the unbound fraction in whole blood and fu_p is the unbound fraction in plasma. Other chemical properties of carbaryl used in the prediction were $\log P_{o:w} = 2.36$ and $pK_a = 10.4$. The fu_p predicted from SimCyp was 0.208, which was almost the same as our rat result and close to that for human plasma. The method used in SimCyp is based on Rodgers et al. (2005) and Rodgers and Rowland (2006, 2007).

Table 4
Physiological and chemical specific parameters used for carbaryl rat PBPK/PD model.

Parameters	Values	Sources
BW	0.25	Nong et al. (2008)
QCC (cardiac output scalar)	15.6	Brown et al. (1997)
Hematocrit (HCT)	0.450	Nong et al. (2008)
Tissue volume (as a fraction of BW)		
Brain (VBRNC)	0.006	Brown et al. (1997)
Fat (VFATC)	0.065	Brown et al. (1997)
Liver (VLIVC)	0.039	Brown et al. (1997)
Blood (VBLDC)	0.065	Brown et al. (1997)
Tissue blood (VTBC, as fraction of tissue volume)	0.050	Brown et al. (1997)
Blood flow (as a fraction of cardiac output)		
Brain (QBRNC)	0.020	Brown et al. (1997)
Fat (QFATC)	0.070	Brown et al. (1997)
Liver (QLIVC)	0.160	Brown et al. (1997)
Rest of body (QBODC)	Difference	1 – QBRNC – QFATC – QLIVC
Basal ChE parameters		
Basal AChE activity in brain (BRACHE)	462,962	Based on in vitro data
Basal AChE activity in plasma (BACHE)	8872	Based on in vitro data
Basal BuChE activity in plasma (BBCHE)	3335	Based on in vitro data
Basal AChE activity in RBCs (RBACHE)	36,050	Based on in vitro data
RBC AChE basal degradation rate constant (KDACHERBC)	0.01	Nong et al. (2008)
Brain AChE basal degradation rate constant (KDACHEBRN)	0.01	Nong et al. (2008)
Plasma AChE basal degradation rate constant (KDACHEPLS)	0.10	Nong et al. (2008)
Plasma BuChE basal degradation rate constant (KDBCHE)	0.10	Nong et al. (2008)
AChE enzyme turnover rate (TRCE)	11,700,000	Wang and Murphy (1982)
BuChE enzyme turnover rate (TRBE)	3,660,000	Main et al. (1972)
Partition coefficient (tissue to plasma)		
Brain to plasma (PBRN)	1.0	Fitted[a]
Fat to plasma (PFAT)	6.0	Fitted[a]
Rest of body to plasma (PBOD)	0.66	Based on in vitro data[b]
Liver to plasma (PLIV)	1.15	Based on in vitro data
RBC to plasma (PRBC)	0.78	Based on in vitro data
Fraction of free carbaryl in the tissue		
Liver (FULIV)	0.17	Based on in vitro data
Brain (FUBRN)	0.39	Based on in vitro data
Plasma (FUp)	0.20	based on in vitro data
RBC (FURBC)	0.25	Based on in vitro data
Tissue permeability-area product for diffusion		
Fat (PAFC)	1.00	Nong et al. (2008)
Rest of body (PARC)	6.29	Nong et al. (2008)
Liver (PALC)	10.0	Fitted[a]
Brain (PABC)	0.13	Nong et al. (2008)
RBC (PARBC)	100	Assumption of rapid diffusion
Metabolic constants		
See Table 1 (based on in vitro data)		
Absorption and intestinal metabolism		
First order gut absorption rate constant (KA)	6.5	Hwang and Schanker (1974)
Fraction absorbed in the gut (FA)	0.5	Fitted[a]
Fraction absorbed in the gut (FM)	0.25	Fitted[a]
ChE interaction parameters		
k_i for RBC AChE (KIACHERBC)[c]	1.34	Based on in vitro data/assumption
k_r for RBC AChE (KRACHERBC)	1.54	Based on in vitro data
k_i for brain AChE (KIACHEBRN)[c]	1.28	Based on in vitro data/assumption
k_r for brain AChE (KRACHEBRN)	2.09	Based on in vitro data
k_i for plasma AChE (KIACHEPLS)	11.10	Based on in vitro data
k_r for plasma AChE (KRACHEPLS)	1.6	Based on in vitro data
k_i for plasma BuChE (KIBCHE)	0.53	Based on in vitro data
k_r for plasma BuChE (KRBCHE)	0.45	Based on in vitro data

[a] These parameter values were fitted using tissue concentration data for carbaryl in Nong et al. (2008). There was a limitation of current in vitro based partition coefficient estimation method for brain and fat. PALC was re-estimated using tissue concentration data after all the partitioning parameters were updated. FA and FM were estimated to have model simulations be consistent with the observed brain concentrations from oral dose experiment.
[b] Value for muscle was used as a surrogate for the value for the rest of body compartment.
[c] The k_i value for RBC and brain AChE were adjusted to fit in vivo ChE depression data (Nong et al., 2008) based on polymeric forms these enzymes are present in the given tissue.

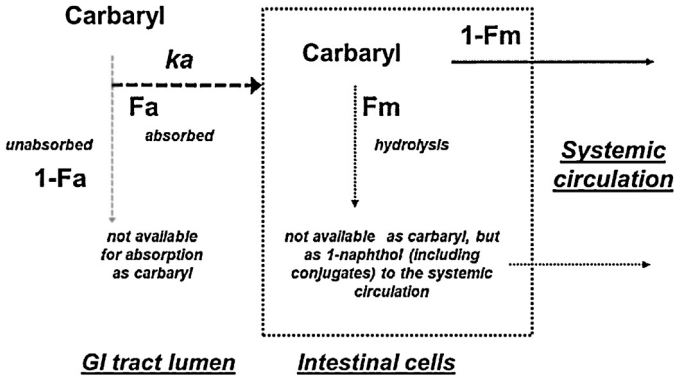

Fig. 7. Description of carbaryl absorption in the gut. The abbreviations are as follows: FA – fraction of the amount of carbaryl in the gut lumen that is absorbed as carbaryl; FM – fraction of the absorbed carbaryl that is metabolized in the gut enterocytes.

3.3.2.2. Extrapolation of ChE binding parameters. Bimolecular inhibition and decarbamylation rate constants were directly incorporated in the model as measured since they describe intensive biochemical processes that are not dependent on the amount of enzyme content present (Table 1). Similarly, the rate constant for chemical degradation of carbaryl was also directly used in the PBPK model (Table 1).

3.4. Performance of the Rat PBPK/PD model for carbaryl

3.4.1.1. Carbaryl kinetics

The performance of the model was first evaluated using the time-course data for tissue carbaryl after the single IV dose. The model was able to simulate the time-dependent changes in carbaryl concentration in the brain and other tissues reasonably well, showing the overall model predictions were within twofold of the observed tissue carbaryl concentration data when the model was parameterized using in vitro-based parameters for metabolism and enzyme inhibition. In addition, the model predicted time course curves were consistent with the observed time profiles of tissue carbaryl concentrations. This agreement provides some confidence in the model assumptions regarding the differential impacts of binding in plasma and thermodynamic partitioning of carbaryl in the tissue on carbaryl availability for diffusion across cellular membranes and for metabolism, as well as for the description of free concentration in the in vitro and in vivo systems.

To simulate carbaryl kinetics after the oral exposure, we used a more detailed gut description than the previously published in vivo data-based model (Nong et al., 2008). The oral bioavailability (FA) in the gut and fraction of absorbed carbaryl that undergoes intestinal metabolism (FM) were estimated to reproduce the observed carbaryl concentrations in brain and 1-naphthol sulfate concentrations in plasma over time after the exposure (Fig. 9).

The model reproduced the time profiles of 1-naphthol sulfate concentration in plasma reasonably well both for IV and oral exposures (Figs. 8 and 9). However, post-exposure plasma concentrations of carbaryl were generally underestimated compared to the data (Fig. 8). Spontaneous degradation of carbaryl during handling and/or storage of the tissue may have occurred, based on our own observation of chemical degradation of carbaryl. Results of another PK study of carbaryl also support this speculation, since the ratio of carbaryl in the brain to that in plasma in that study was close to unity over a wide range of doses (Herr et al., 2010), in agreement with our model predictions.

3.4.1.2. Interaction with ChEs

Despite the good agreement between the model and the data for tissue concentrations, our model tended to overestimate, by up to a factor of two, the extent of AChE inhibition in brain and RBCs if in vitro measured parameters were used directly (Fig. 10). This leads us to consider additional factors that might need to be considered when extrapolating in vitro determined inhibition rate constants for ChEs. If the in vitro-determined k_i value was adjusted by the number of monomers in the respective multimeric AChE enzymes in the brain or RBCs (Tables 2 and 5), 4 for brain and 2 for RBCs, better agreement was achieved between the model-simulated and measured time profiles of ChE inhibition by carbaryl (Fig. 10).

3.4.1.3. Sensitivity analysis

Sensitivity analysis evaluated the influence of the model parameters on the concentration of carbaryl in the brain (Table 5). The list of parameters with SCs greater than 0.2, which is considered sensitive parameters for brain carbaryl concentration, included partitioning to the liver and brain; tissue volumes and blood flows to the brain and liver; and hepatic metabolism. This indicates that both the distribution and metabolism are important in determining the brain concentration at the selected time point. In addition, FM and FA, which determine the oral bioavailability of carbaryl showed appreciable sensitivities to the brain concentration as expected.

4. Discussion

Our study evaluated the use in vitro determined biochemical constants to provide chemical specific in vivo parameters in PBPK models. The results of this case study with carbaryl indicate that the success of IVIVE is largely dependent on (1) a thorough characterization of in vitro experimental system and (2) a proper PBPK model structure/parameters that allows the in vivo description to be linked with its in vitro counterpart. Our ultimate goal is to provide a tool that can use in vitro information to support human risk assessment of environmental compounds. To this end, this study showed how the parallelogram approach can help better design human in vitro studies and thus provide a firm basis for IVIVE-based human PBPK models (Yoon et al., 2012b). In this study, several assumptions were evaluated for IVIVE of kinetic parameters using the rat carbaryl model as a case study. Human in vitro studies were presented in this paper as well to show how the rat in vitro studies helped design those studies and interpret the results from them. The human carbaryl model will be described in a separate paper (Holm et al., 2013).

One of the major issues in extrapolating in vitro-derived parameters for PK and PD models is the relevance of the compound concentrations used to obtain concentration-dependent parameters, both in vitro and in vivo (Blaauboer, 2010). Since biochemical reactions in the cell – such as metabolism or binding to target receptors/proteins – are dependent on the free concentration of the compound, in vitro derived affinity constants will be greatly affected if not properly adjusted for factors affecting free concentration. To define the free concentration of carbaryl in the tissue (intracellular compartment) in vivo, both the tissue to plasma partition coefficients and the unbound fraction were used in the model. The unbound fraction was used to describe the available carbaryl concentration for metabolism and binding to ChEs in the liver, brain, plasma and RBCs appropriately. We assumed that the diffusional exchange of carbaryl between the plasma and tissue (including RBCs) was rapid, and not limited by binding to plasma proteins. Tissue partitioning was taken as a measure of thermodynamic equilibration of carbaryl between the tissue matrix and plasma, but only the free concentration governs

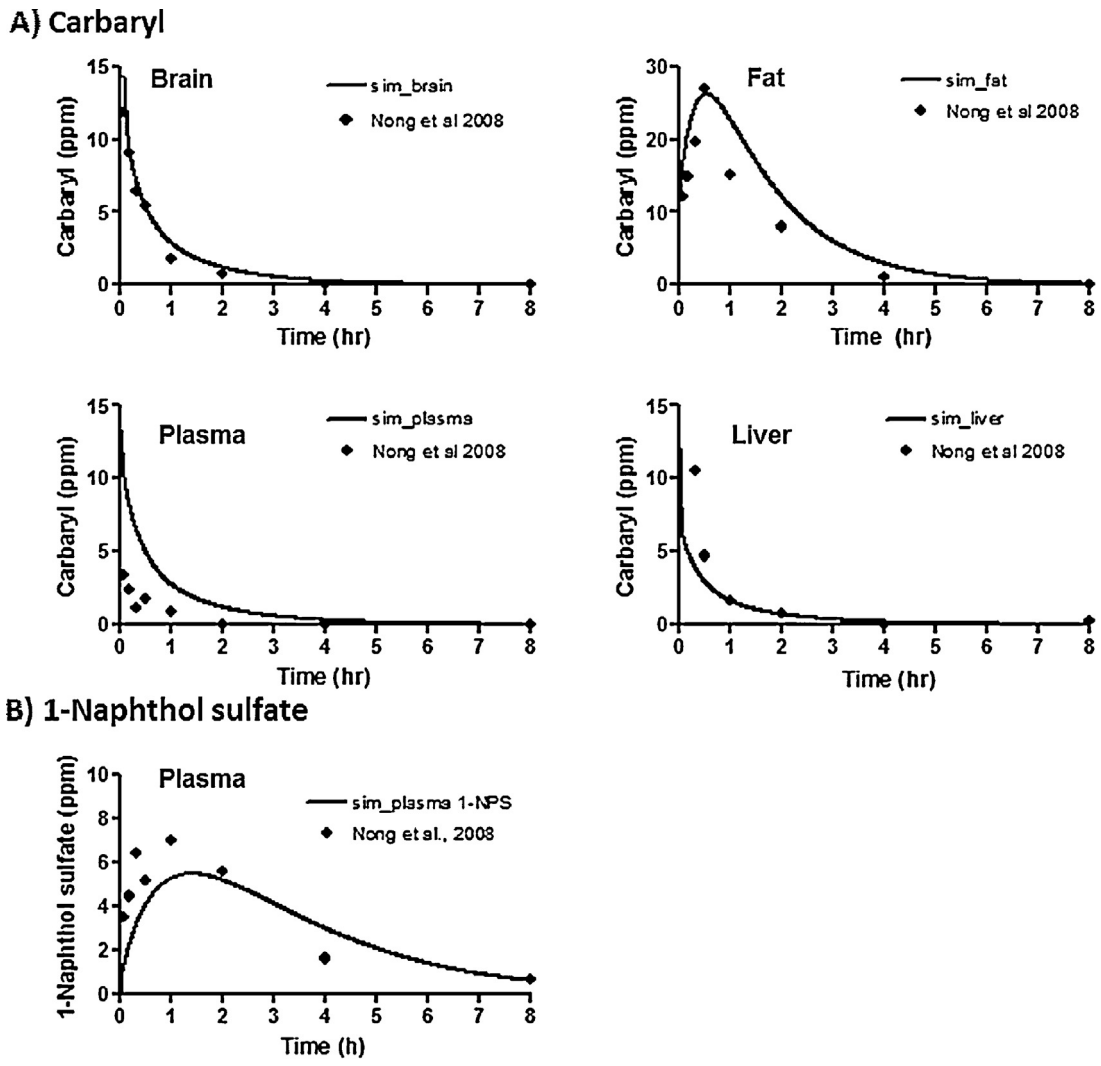

Fig. 8. Modeling of single IV study in adult rats. Symbols represent the carbaryl concentration measured in one pooled tissue sample from 4 animals, whereas lines represent model simulations for carbaryl tissue concentrations after the single IV dose (9.2 mg/kg).

carbaryl availability in the aqueous region of the tissue where enzyme–substrate interactions occur. It should be emphasized again that biochemical parameters were measured and expressed based on the free concentration in vitro to the extent possible. They were extrapolated to each corresponding parameter in vivo in terms of the free concentration in the given environment.

Experimental determination of tissue to blood partition coefficients for non-volatile compounds can be challenging, despite the fact that a number of different methods are available (Basketter et al., 2012). Each method has its own limitation which usually involves non-specific binding to the assay vessels and/or deterioration of tissue matrix leading to incorrect estimation of free concentration in the given tissue. Our attempt to use in vitro binding data to inform in vivo tissue partitioning showed the limitations of this approach in its current form. The greater discrepancies for brain and fat PCs compared to the in vivo-based estimates

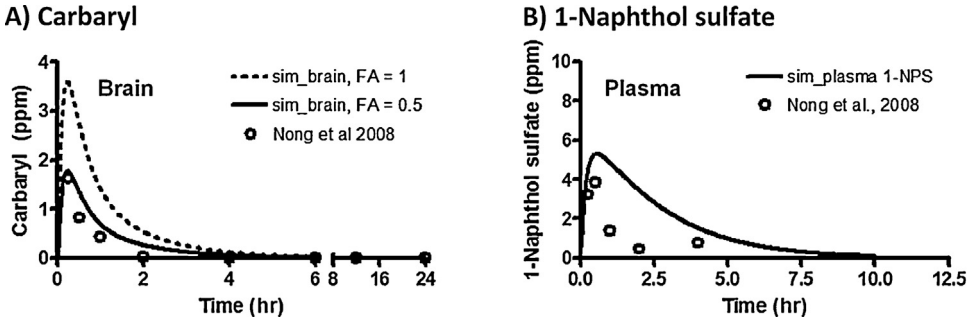

Fig. 9. Modeling of single oral Evaluation of model performance using the data from the single oral dose study. Symbols represent the carbaryl concentration measured in one pooled tissue sample from 4 animals, whereas lines represent model simulations for carbaryl tissue concentrations after the single oral dose (8.45 mg/kg). Two different FA values were used for comparison in the case of brain.

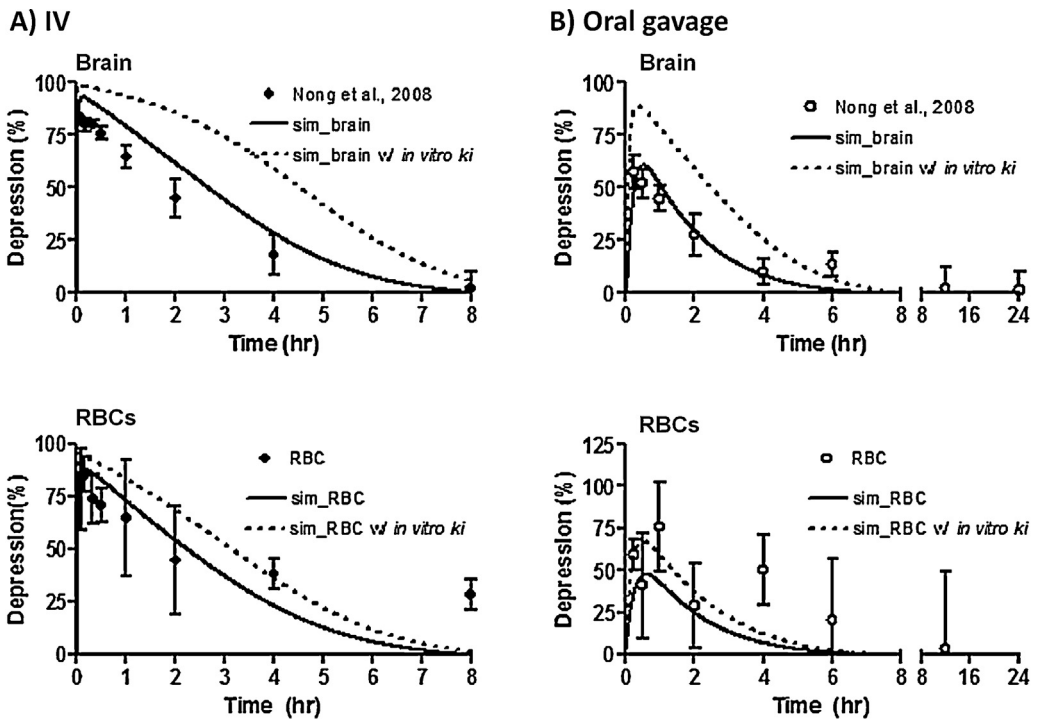

Fig. 10. Time course of ChE inhibition in the brain and RBCs by carbaryl. Symbols represent the mean ± SD for % depression of ChE in each tissue compared to control from 4 individual animals, whereas lines represent model simulations with appropriately adjusted k_i (solid lines) or in vitro-derived k_i directly incorporated in the model (dotted lines).

may be attributable to the dialysis conditions, where tissues were homogenized in aqueous buffer and incubated for extended periods of time. Loss of homogeneity in the tissue homogenate could have been greater for these high lipid containing tissues compared to other tissues. Overall, our case study suggests that predicting tissue partitioning and, therefore, volume of distribution of a compound may be a major challenge in IVIVE.

A key conclusion of this case study is the need for the development of methods for estimating GI absorption kinetics and metabolism. Evaluation of the model performance with IV data provides confidence in the in vitro-based parameters for distribution and metabolism of carbaryl. With the revised GI description which includes bioavailability and intestinal metabolism terms, better agreement was achieved between the data and model simulations for oral dosing. Based on our estimates, 50% of orally administered carbaryl appears to be absorbed into the systemic circulation as carbaryl and about 30% of the absorbed carbaryl is metabolized in the gut epithelial cells (Table 4). Although evidence for intestinal metabolism of carbaryl is a matter of debate (Houston et al., 1975; Pekas, 1980), the presence of CYP3A4 in the gut (Paine et al., 2006; Shen et al., 1997), one of the CYP isoforms responsible for carbaryl metabolism, (Tang et al., 2002), and the evidence for hydrolysis of ester-compounds in the gut (Imai et al., 2005), indicate the potential role of intestinal metabolism in carbaryl bioavailability. Methods have been developed for estimating the bioavailability and pre-hepatic metabolism of drugs; however, these methods are semi-empirical, relying on regressions of in vivo data for a number of drug compounds. It has not yet been demonstrated that data from drug-like compounds can be used to estimate the kinetics and metabolism of environmental compounds with much more variable physicochemical and biochemical characteristics (Yoon et al., 2012a).

Table 5
Sensitivity of carbaryl model parameters for 40 min post-exposure carbaryl concentrations in the brain.

	Parameter description	IV	Oral
		9.2 mg/kg Sensitivity coefficient	8.45 mg/kg
Physiological parameters	Liver volume (VLIVC)	**−0.46**	**−0.69**
	Fat volume (VFATC)	**−0.24**	−0.11
	Liver blood flow (QLIVC)	**−0.39**	0.13
	Cardiac output (QCC)	**−0.37**	0.13
	Hematocrit (HCT)	**0.33**	−0.03
Carbaryl-specific Parameters	Brain to plasma PC (PBRN)	**1.04**	**1.03**
	Liver to plasma PC (PLIV)	**−0.40**	**−0.69**
	Fraction free in the liver (FULIV)	**−0.45**	**−0.70**
	CL_{int} for liver oxidative metabolism (CL_{rat1})	**−0.77**	**−0.52**
	Fraction metabolized in the gut (FM)	n/a[a]	**−0.34**
	Fraction absorbed in the gut (FA)	n/a[a]	**1.01**

Sensitivity coefficients greater than 0.2 for any of the selected dose metrics in either of the two dosing regimens are displayed. Sensitivity coefficients smaller than 0.2 are deemed insignificant according to the criteria used in Yoon et al. (2009).

[a] Not applicable for IV dose.

Considering the tissue-specific oligomeric conformations of ChEs (Aldunate et al., 2004; Skau, 1985), the observed variation in k_i values among tissues seems to be reasonable. While the accessibility of carbaryl to ChEs could be affected by different conformations, liberation of carbaryl from the already carbamylated enzyme would be expected to occur in a similar manner regardless of conformation. The tendency for overestimation of AChE inhibition in the brain and RBCs may be attributable to slight conformational changes of this ologomeric enzyme, possibly occurring during sample preparation, especially during homogenization and dilution of the tissue. AChE is present as a tetramer anchored to the synaptic membrane in the brain, while it is predominantly in a dimeric form in mammalian RBCs (Aldunate et al., 2004; Roberts et al., 1987; Skau, 1985). This hypothesis was supported by the improved consistency between the data and model simulations for ChE depression after taking this possibility into account during extrapolation. Other impacts of experimental conditions on k_i measurement cannot be ruled out, however. It has been a matter of debate whether or to what extent non-specific binding of inhibitors, e.g., carbamates or organophosphates, to lipids or proteins in tissue homogenates could explain the variation in determined k_i values (Kousba et al., 2007).

In addition to the immediate value in providing an estimate of average metabolic clearance in vivo, as demonstrated in this study, in vitro data can also help address human variability and/or potentially sensitive subpopulation in risk assessment by integrating data from small scale in vitro studies with pooled samples or samples from a limited number of individuals with other in vitro based information that can reflect variability at a population level. If a single metabolic enzyme is (largely) responsible for the clearance of a given compound, it is highly probable that the variability in hepatic clearance is determined by the differences in expression of that specific enzyme/isoform among individuals. A strong correlation has been shown between CYP2E1 expression and trichloroethylene activation to chloral hydrate in human microsomes among individual donors (Snawder and Lipscomb, 2000). No such correlation, however, was observed between trichloroethylene metabolism and total microsomal CYP content (Lipscomb et al., 1997). The fact that the carbaryl CL_{int} at low concentration was not affected by 1-ABT, along with the good correlation with ECOD activity, implies that at the exposure levels expected for humans, carbaryl metabolism may be dependent on total CYP content rather than one or two specific isoforms. Involvement of multiple CYPs including CYP3A4, CYP1A1, CYP1A2, and CYP2B6 was reported using human liver microsomes and recombinant CYP isoforms (Tang et al., 2002). These CYP enzymes constitute the major contributors to total human liver P450 activity (Shimada et al., 1994) and therefore, would be expected to contribute collectively to total carbaryl clearance and hence, to population variability in the hepatic clearance of carbaryl.

Clearance of carbaryl in plasma in humans was much greater than in adult SD rats (Table 1). This observation is consistent with the findings from studies in human volunteers that suggested 1-naphthol and its conjugates are the major metabolites of carbaryl in humans (Knaak et al., 1968). Our results suggest a significant involvement of Ca^{2+} dependent A-esterase (PON) activity in human plasma. From the perspective of risk assessment, potential impacts of the PON polymorphism on carbaryl metabolism in plasma might be one factor to consider in addressing potentially sensitive subpopulations. As BuChE inhibition by carbaryl is a one-to-one stoichiometric process that eventually hydrolyses carbaryl, the observed lack of impact of a BuChE inhibitor on carbaryl clearance in plasma indicates that this enzyme may not be an efficient 'trapping' agent for carbaryl.

In conclusion, the results of this case study indicate that extrapolation of in vitro-derived metabolic parameters can predict in vivo pharmacokinetics and pharmacodynamics, but careful consideration of free concentrations, both in vitro and in vivo, is necessary. Moreover, predicting tissue partitioning from in vitro information can still be challenging. Estimation of pre-hepatic clearance in the gut was identified as one of the key deficiencies in current approaches for IVIVE-based prediction of in vivo kinetics. Further research efforts are also needed on the development of improved experimental tools for estimating in vivo kinetic parameters with in vitro assays, as well as on a generalized PBPK modeling platform for environmental compounds that has the capability to properly utilize in vitro based information to conduct IVIVE for environmental risk assessments, similar to the Simcyp program for pharmaceutical compounds. Overall, we believe our proposed IVIVE-based PBPK model parameterization approach will be of considerable value for broad implementation of PBPK models in human health risk assessment under any new in vitro toxicity testing paradigm.

Funding

The experimental research on carbaryl was supported by a Cooperative Research and Development Agreement between the United States Environmental Protection Agency and The Hamner Institutes for Health Sciences (EPA Grant Number: R833452). The QIVIVE carbaryl case study application was funded by the American Chemistry Council Long-Range Research Initiative.

Conflict of interest

The authors declare that there are no conflicts of interest.

Transparency document

The Transparency document associated with this article can be found in the online version.

Acknowledgements

The authors would like to thank Dr. John Lipscomb for his helpful comments on the potential impact of total CYP content on variability in metabolism across individuals and Mr. David Billings for his help in simplifying the code for 1-naphthol compartment, formatting the manuscript and organizing references.

References

Aldunate, R., Casar, J.C., Brandan, E., Inestrosa, N.C., 2004. Structural and functional organization of synaptic acetylcholinesterase. Brain Res. Brain Res. Rev. 47, 96–104.

Andersen, M.E., Krewski, D., 2010. The vision of toxicity testing in the 21st century: moving from discussion to action. Toxicol. Sci. 117, 17–24.

Barter, Z.E., Bayliss, M.K., Beaune, P.H., Boobis, A.R., Carlile, D.J., Edwards, R.J., Houston, J.B., Lake, B.G., Lipscomb, J.C., Pelkonen, O.R., Tucker, G.T., Rostami-Hodjegan, A., 2007. Scaling factors for the extrapolation of in vivo metabolic drug clearance from in vitro data: reaching a consensus on values of human microsomal protein and hepatocellularity per gram of liver. Curr. Drug Metab. 8, 33–45.

Barton, H.A., Chiu, W.A., Woodrow Setzer, R., Andersen, M.E., Bailer, A.J., Bois, F.Y., Dewoskin, R.S., Hays, S., Johanson, G., Jones, N., Loizou, G., Macphail, R.C., Portier, C.J., Spendiff, M., Tan, Y.M., 2007. Characterizing uncertainty and variability in physiologically based pharmacokinetic models: state of the science and needs for research and implementation. Toxicol. Sci. 99, 395–402.

Basketter, D.A., Clewell, H., Kimber, I., Rossi, A., Blaauboer, B.J., Burrier, R., Daneshian, M., Eskes, C., Goldberg, A., Hasiwa, N., Hoffman, S., Jaworska, J., Knudsen, T.B., Landsiedel, R., Leist, M., Locke, P., Maxwell, G., McKim, J., McVey, E.A., Ouedraogo, G., Patlewicz, G., Pelkonen, O.R., Roggen, E., Rovida, C., Ruhdel, I., Schwarz, M., Schepky, A., Schoeters, G., Skinner, N., Trentz, K., Turner, M., Vanparys, P., Yager, J., Zurlo, J., Hartung, T.A., 2012. Roadmap for the development of alternative (non-animal) methods for systemic toxicity testing – t4 report*. ALTEX 29, 3–91.

Blaauboer, B.J., 2010. Biokinetic modeling and in vitro–in vivo extrapolations. J. Toxicol. Environ. Health B: Crit. Rev. 13, 242–252.

Brownson, C., Watts, D.C., 1973. The modification of cholinesterase activity by 5,5′-dithiobis-(2-nitrobenzoic acid) included in the coupled spectrophotometric

assay. Evidence for a non-catalytic substrate-binding site. Biochem. J. 131, 369–374.
Brown, R., Delp, M., Lindstedt, S., Rhomberg, L., Beliles, R., 1997. Physiological parameter values for physiologically based pharmacokinetic models. Toxicol. Ind. Health 13407, 484.
Copeland, R.A., 2002. Tight Binding Inhibitors, Enzymes. John Wiley & Sons Inc., New York, pp. 305–317.
Ellman, G.L., Courtney, K.D., Andres Jr., V., Feather-Stone, R.M., 1961. A new and rapid colorimetric determination of acetylcholinesterase activity. Biochem. Pharmacol. 7, 88–95.
Floby, E., Johansson, J., Hoogstraate, J., Hewitt, N.J., Hill, J., Sohlenius-Sternbeck, A.K., 2009. Comparison of intrinsic metabolic clearance in fresh and cryopreserved human hepatocytes. Xenobiotica 39, 656–662.
Groner, E., Ashani, Y., Schorer-Apelbaum, D., Sterling, J., Herzig, Y., Weinstock, M., 2007. The kinetics of inhibition of human acetylcholinesterase and butyrylcholinesterase by two series of novel carbamates. Mol. Pharmacol. 71, 1610–1617.
Herr, D.W., Mwanza, J.C., Lyke, D.F., Graff, J.E., Moser, V.C., Padilla, S., 2010. Relationship between brain and plasma carbaryl levels and cholinesterase inhibition. Toxicology 276, 172–183.
Holm, K., McDougall, R., Yoon, M., Young, B., Clewell, H., Tornero-Velez, R., Goldsmith, R., Chang, D., Grulke, C., Phillips, M., Dary, C., Tan, C., 2013. Identifying the sources of uncertainty in the process of reconstructing exposures to carbaryl using exposure-to-dose modeling. Toxicologist 132, 171.
Houston, J.B., Upshall, D.G., Bridges, J.W., 1975. Pharmacokinetics and metabolism of two carbamate insecticides, carbaryl and landrin, in the rat. Xenobiotica 5, 637–648.
Hwang, S.W., Schanker, L.S., 1974. Absorption of carbaryl from the lung and small intestine of the rat. Environ. Res. 7, 206–211.
Imai, T., Imoto, M., Sakamoto, H., Hashimoto, M., 2005. Identification of esterases expressed in Caco-2 cells and effects of their hydrolyzing activity in predicting human intestinal absorption. Drug Metab. Dispos. 33, 1185–1190.
Judson, R.S., Kavlock, R.J., Setzer, R.W., Hubal, E.A., Martin, M.T., Knudsen, T.B., Houck, K.A., Thomas, R.S., Wetmore, B.A., Dix, D.J., 2011. Estimating toxicity-related biological pathway altering doses for high-throughput chemical risk assessment. Chem. Res. Toxicol. 24, 451–462.
Kalvass, J.C., Maurer, T.S., 2002. Influence of nonspecific brain and plasma binding on CNS exposure: implications for rational drug discovery. Biopharm. Drug Dispos. 23, 327–338.
Kedderis, G.L., 2007. In vitro to in vivo extrapolation of metabolic rate constants for physiologically based pharmacokinetic models. In: Lipscomb, J.C., Ohanian, E.V. (Eds.), Toxicokinetics and Risk Assessment. Informa Healthcare, New York, pp. 185–210.
Kedderis, G.L., Argenbright, L.S., Miwa, G.T., 1988. Studies with nitrogen-containing steroids and freshly isolated rat hepatocytes: role of cytochrome P-450 in detoxication. Toxicol. Appl. Pharmacol. 93, 403–412.
Kedderis, G.L., Held, S.D., 1996. Prediction of furan pharmacokinetics from hepatocyte studies: comparison of bioactivation and hepatic dosimetry in rats, mice, and humans. Toxicol. Appl. Pharmacol. 140, 124–130.
Knaak, J.B., Tallant, M.J., Kozbelt, S.J., Sullivan, L.J., 1968. The metabolism of carbaryl in man, monkey, pig, and sheep. J. Agric. Food Chem. 16, 465–470.
Knudsen, T.B., Houck, K.A., Sipes, N.S., Singh, A.V., Judson, R.S., Martin, M.T., Weissman, A., Kleinstreuer, N.C., Mortensen, H.M., Reif, D.M., Rabinowitz, J.R., Setzer, R.W., Richard, A.M., Dix, D.J., Kavlock, R.J., 2011. Activity profiles of 309 ToxCast chemicals evaluated across 292 biochemical targets. Toxicology 282, 1–15.
Kousba, A.A., Poet, T.S., Timchalk, C., 2003. Characterization of the in vitro kinetic interaction of chlorpyrifos-oxon with rat salivary cholinesterase: a potential biomonitoring matrix. Toxicology 188, 219–232.
Kousba, A.A., Poet, T.S., Timchalk, C., 2007. Age-related brain cholinesterase inhibition kinetics following in vitro incubation with chlorpyrifos-oxon and diazinon-oxon. Toxicol. sci. 95, 147–155.
Lipscomb, J.C., Garrett, C.M., Snawder, J.E., 1997. Cytochrome P450-dependent metabolism of trichloroethylene: interindividual differences in humans. Toxicol. Appl. Pharmacol. 142, 311–318.
Lipscomb, J.C., Poet, T.S., 2008. In vitro measurements of metabolism for application in pharmacokinetic modeling. Pharmacol. Ther. 118, 82–103.
Main, A.R., 1969. Kinetics of cholinesterase inhibition by organophosphate and carbamate insecticides. Can. Med. Assoc. J. 100, 161–167.
Maxwell, D.M., Lenz, D.E., Groff, W.A., Kaminskis, A., Froehlich, H.L., 1987. The effects of blood flow and detoxification on in vivo cholinesterase inhibition by soman in rats. Toxicol. Appl. Pharmacol. 88, 66–76.
McCracken, N.W., Blain, P.G., Williams, F.M., 1993. Nature and role of xenobiotic metabolizing esterases in rat liver, lung, skin and blood. Biochem. Pharmacol. 45, 31–36.
McDaniel, K.L., Padilla, S., Marshall, R.S., Phillips, P.M., Podhorniak, L., Qian, Y., Moser, V.C., 2007. Comparison of acute neurobehavioral and cholinesterase inhibitory effects of N-methylcarbamates in rat. Toxicol. Sci. 98, 552–560.
McGinnity, D.F., Soars, M.G., Urbanowicz, R.A., Riley, R.J., 2004. Evaluation of fresh and cryopreserved hepatocytes as in vitro drug metabolism tools for the prediction of metabolic clearance. Drug Metab. Dispos. 32, 1247–1253.
Nong, A., Tan, Y.M., Krolski, M.E., Wang, J., Lunchick, C., Conolly, R.B., Clewell 3rd, H.J., 2008. Bayesian calibration of a physiologically based pharmacokinetic/pharmacodynamic model of carbaryl cholinesterase inhibition. J. Toxicol. Environ. Health A 71, 1363–1381.
Nostrandt, A.C., Duncan, J.A., Padilla, S., 1993. A modified spectrophotometric method appropriate for measuring cholinesterase activity in tissue from carbaryl-treated animals. Fundam. Appl. Toxicol. 21, 196–203.
Padilla, S., 1995. Regulatory and research issues related to cholinesterase inhibition. Toxicology 102, 215–220.
Paine, M.F., Hart, H.L., Ludington, S.S., Haining, R.L., Rettie, A.E., Zeldin, D.C., 2006. The human intestinal cytochrome P450 "pie". Drug Metab. Dispos. 34, 880–886.
Pekas, J.C., 1980. Gastrointestinal metabolism and transport of pesticidal carbamates. Crit. Rev. Toxicol. 7, 37–101.
Roberts, W.L., Kim, B.H., Rosenberry, T.L., 1987. Differences in the glycolipid membrane anchors of bovine and human erythrocyte acetylcholinesterases. Proc. Natl. Acad. Sci. U. S. A. 84, 7817–7821.
Rodgers, T., Leahy, D., Rowland, M., 2005. Physiologically based pharmacokinetic modeling 1: predicting the tissue distribution of moderate-to-strong bases. J. Pharm. Sci. 94, 1259–1276.
Rodgers, T., Rowland, M., 2006. Physiologically based pharmacokinetic modeling 2: predicting the tissue distribution of acids, very weak bases, neutrals and zwitterions. J. Pharm. Sci. 95, 1238–1257.
Rodgers, T., Rowland, M., 2007. Mechanistic approaches to volume of distribution predictions: Understanding the processes. Pharm. Res. 24, 918–933.
Rotroff, D.M., Wetmore, B.A., Dix, D.J., Ferguson, S.S., Clewell, H.J., Houck, K.A., Lecluyse, E.L., Andersen, M.E., Judson, R.S., Smith, C.M., Sochaski, M.A., Kavlock, R.J., Boellmann, F., Martin, M.T., Reif, D.M., Wambaugh, J.F., Thomas, R.S., 2010. Incorporating human dosimetry and exposure into high-throughput in vitro toxicity screening. Toxicol. Sci. 117, 348–358.
Shen, D.D., Kunze, K.L., Thummel, K.E., 1997. Enzyme-catalyzed processes of first-pass hepatic and intestinal drug extraction. Adv. Drug Deliv. Rev. 27, 99–127.
Shimada, T., Tsumura, F., Yamazaki, H., 1999. Prediction of human liver microsomal oxidations of 7-ethoxycoumarin and chlorzoxazone with kinetic parameters of recombinant cytochrome P-450 enzymes. Drug Metab. Dispos. 27, 1274–1280.
Shimada, T., Yamazaki, H., Mimura, M., Inui, Y., Guengerich, F.P., 1994. Interindividual variations in human liver cytochrome P-450 enzymes involved in the oxidation of drugs, carcinogens and toxic chemicals: studies with liver microsomes of 30 Japanese and 30 Caucasians. J. Pharmacol. Exp. Ther. 270, 414–423.
Skau, K.A., 1985. Acetylcholinesterase molecular forms in serum and erythrocytes of laboratory animals. Comp. Biochem. Physiol. C 80, 207–210.
Snawder, J.E., Lipscomb, J.C., 2000. Interindividual variance of cytochrome P450 forms in human hepatic microsomes: correlation of individual forms with xenobiotic metabolism and implications in risk assessment. Regul. Toxicol. Pharmacol. 32, 200–209.
Sogorb, M.A., Vilanova, E., 2002. Enzymes involved in the detoxification of organophosphorus, carbamate and pyrethroid insecticides through hydrolysis. Toxicol. Lett. 128, 215–228.
Sohlenius-Sternbeck, A.K., 2006. Determination of the hepatocellularity number for human, dog, rabbit, rat and mouse livers from protein concentration measurements. Toxicol. In Vitro 20, 1582–1586.
Tang, J., Cao, Y., Rose, R.L., Hodgson, E., 2002. In vitro metabolism of carbaryl by human cytochrome P450 and its inhibition by chlorpyrifos. Chem. Biol. Interact. 141, 229–241.
Tang, J., Chambers, J.E., 1999. Detoxication of paraoxon by rat liver homogenate and serum carboxylesterases and A-esterases. J. Biochem. Mol. Toxicol. 13, 261–268.
Wang, C., Murphy, S., 1982. The role of non-critical binding proteins in the sensitivity of acetylcholin-esterase from different species to diisopropyl fluorophosphate (DFP), in vitro. Life sci. 31, 139–149.
Waxman, D.J., Lapenson, D.P., Aoyama, T., Gelboin, H.V., Gonzalez, F.J., Korzekwa, K., 1991. Steroid hormone hydroxylase specificities of eleven cDNA-expressed human cytochrome P450s. Arch. Biochem. Biophys. 290, 160–166.
Wetmore, B.A., Wambaugh, J.F., Ferguson, S.S., Sochaski, M.A., Rotroff, D.M., Freeman, K., Clewell 3rd, H.J., Dix, D.J., Andersen, M.E., Houck, K.A., Allen, B., Judson, R.S., Singh, R., Kavlock, R.J., Richard, A.M., Thomas, R.S., 2012. Integration of dosimetry, exposure, and high-throughput screening data in chemical toxicity assessment. Toxicol. Sci. 125, 157–174.
Yan, G.Z., Brouwer, K.L., Pollack, G.M., Wang, M.Z., Tidwell, R.R., Hall, J.E., Paine, M.F., 2011. Mechanisms underlying differences in systemic exposure of structurally similar active metabolites: comparison of two preclinical hepatic models. J. Pharmacol. Exp. Ther. 337, 503–512.
Yan, G.Z., Generaux, C.N., Yoon, M., Goldsmith, R.B., Tidwell, R.R., Hall, J.E., Olson, C.A., Clewell, H.J., Brouwer, K.L., Paine, M.F., 2012. A semiphysiologically based pharmacokinetic modeling approach to predict the dose-exposure relationship of an antiparasitic prodrug/active metabolite pair. Drug Metab. Dispos. 40, 6–17.
Yoon, M., Campbell, J.L., Andersen, M.E., Clewell, H.J., 2012a. Quantitative in vitro to in vivo extrapolation of cell-based toxicity assay results. Crit. Rev. Toxicol. 42, 633–652.
Yoon, M., Kedderis, G.L., Yang, Y., Allen, B.C., Yan, G.Z., Clewell, H.J., 2012b. Use of in vitro data in PBPK models: an example of in vitro to in vivo extrapolation with carbaryl. In: Parameters for Pesticide ASQR and PBPK/PD Models for Human Risk Assessment. American Chemical Society, pp. 323–338.
Yoon, M., Nong, A., Clewell 3rd, H.J., Taylor, M.D., Dorman, D.C., Andersen, M.E., 2009. Evaluating placental transfer and tissue concentrations of manganese in the pregnant rat and fetuses after inhalation exposures with a PBPK model. Toxicol. Sci. 112, 44–58.